Philosophical Magazine
Publication details, including instructions for authors and subscription information:
http://www.tandfonline.com/loi/tphm20

Phase field modelling of grain boundary motion driven by curvature and stored energy gradients. Part II: Application to recrystallisation

G. Abrivard [a], E.P. Busso [a], S. Forest [a] & B. Appolaire [b]

[a] Centre des Matériaux, Mines ParisTech/CNRS UMR 7633, BP 87, 91003 Evry cedex, France

[b] LEM, ONERA/CNRS UMR 104, 29 Av. Division Leclerc, BP 72, 92322 Châtillon, France

Version of record first published: 17 Sep 2012.

To cite this article: G. Abrivard, E.P. Busso, S. Forest & B. Appolaire (2012): Phase field modelling of grain boundary motion driven by curvature and stored energy gradients. Part II: Application to recrystallisation, Philosophical Magazine, 92:28-30, 3643-3664

To link to this article: http://dx.doi.org/10.1080/14786435.2012.717726

Philosophical Magazine
Vol. 92, Nos. 28–30, 1–21 October 2012, 3643–3664

Taylor & Francis
Taylor & Francis Group

Phase field modelling of grain boundary motion driven by curvature and stored energy gradients. Part II: Application to recrystallisation

G. Abrivard[a], E.P. Busso[a]*, S. Forest[a] and B. Appolaire[b]

[a]*Centre des Matériaux, Mines ParisTech/CNRS UMR 7633, BP 87, 91003 Evry cedex, France;* [b]*LEM, ONERA/CNRS UMR 104, 29 Av. Division Leclerc, BP 72, 92322 Châtillon, France*

(*Received 2 December 2011; final version received 20 July 2012*)

In this work, the coupled phase field–crystal plasticity constitutive framework proposed in a companion publication [G. Abrivard, E.P. Busso, S. Forest and B. Apolaire, Phil. Mag. (2012) (this issue)] is applied to study the microstructural evolution driven by grain boundary curvature and/or stored energy. Different microstructures involving bicrystals and polycrystals of pure Al are studied and the results compared against experimental data and known analytical solutions. First, the study of a bicrystal with only curvature as the driving force for boundary migration enables the model to reproduce the different mobilities between low and high angle grain boundaries in the absence of Σ-type boundaries, and to identify the threshold misorientation below which the mobility is negligible. The growth of a small dislocation-free grain embedded within a highly deformed one is considered having both curvature and stored energy as the competing driving forces. A parametric study enabled the effect of the initial size of the nucleus on the minimum level of stored energy required for grain migration to be quantified. Finally, a study of recrystallisation and grain growth phenomena on a representative polycrystal aggregate revealed that grains with the lowest stored energy are dominant at the end of the recrystallisation process. The predicted recrystallised material volume fraction evolution and the kinetics of recrystallisation and grain growth were found to have the same dependence on deformation levels and temperature as those reported in the literature. Several outstanding modelling issues are identified and suggestions for further developments are discussed.

Keywords: phase field; recrystallisation; mobile interfaces; theory and modelling

1. Introduction

The understanding and prediction of recrystallisation phenomena in metal-forming processes is crucial for accurate control of the mechanical properties of the resulting components and for their optimisation. Recrystallisation can happen during the deformation *per se*, that is 'dynamically', or it can occur 'statically' driven by thermal activation after the material has been cold worked. Static recrystallisation develops in two stages: first recrystallisation nuclei appear in the highly deformed material,

*Corresponding author. Email: esteban.busso@ensmp.fr

ISSN 1478–6435 print/ISSN 1478–6443 online

http://dx.doi.org/10.1080/14786435.2012.717726
http://www.tandfonline.com

leading to a fine grained microstructure. This is followed by grain growth, which is driven by the need of the microstructure to minimise its total free energy. Two types of energies are responsible for grain boundary motion: an excess of energy due to the highly disordered nature of the grain boundary itself, and the difference between the free energy stored in adjacent grains during deformation. Each of these two energy contributions acts in a different way. When recrystallisation nuclei appear, their kinetics is controlled first by the curvature of the grain boundary, and then by the stored energies. However, even though the minimisation of these energies provides the main recrystallisation driving force, it is the heterogeneity of the microstructure itself which initially controls the development and growth of newly recrystallised grains [1]. As grain boundary migration takes place at the expense of the annihilation of dislocations and point defects, recrystallised microstructures are made up of small grains relatively free of dislocations.

Ideally, the prediction of recrystallisation requires an approach able to reproduce qualitatively and quantitatively physical phenomena associated with (i) the nucleation of new grains, and (ii) the motion of grain boundaries. A large number of different approaches have been proposed so far to describe both stages. Besides the classical empirical Johnson–Mehl–Avrami description [2], the simplest models which incorporate physical mechanisms rely on a mean field approach [3]: they describe the microstructure in terms of average quantities and features (typically grain size and dislocations density). Despite their success in identifying general trends and relevant parameters, they rely on too many simplifying assumptions concerning the morphology of grains and their spatial arrangements to be sufficiently versatile. To overcome these limitations, many approaches have been developed to describe the processes accounting for a detailed description of grain boundary migration: Monte Carlo [4,5], cellular automata [6–8], vertex techniques [9,10], level set [11] and phase field methods [12–14]. If the first three techniques are conceptually simple and easy to implement, their full coupling to mechanics is delicate and resorts to rather complex algorithms (e.g. [15]). On the contrary, level set and phase field methods can be coupled to mechanics in a transparent way following the same numerical technique. Nevertheless, only the phase field approach provides a unified and thermodynamically consistent framework. For a discussion of the different phase field models for grain growth and recrystallisation, the reader is referred to the companion paper [16].

However, despite the crucial role of crystallographic slip in the evolution of the dislocation network, and hence of the stored strain energy, the description of the constitutive material behaviour has generally been based on either simply elastic assumptions or on simplified assumptions whereby the relation between the stored energy and the dislocation network in the deformed microstructure is approximated in an indirect way [17,18]. For instance, in the case of well-defined equiaxed subgrains, the stored energy may be estimated from the subgrain diameter and the specific energy of low angle grain boundaries [1]. It was only recently [16,19] that the important role of the dislocation network on the stored strain energy gradients was explicitly accounted for in the formulation of the driving force for grain growth and recrystallisation. The main objective of this work is therefore to study recrystallisation phenomena using the more rigorous continuum description of deformation phenomena presented in the coupled phase field-crystal plasticity approach of [16].

It is worth pointing out that the main original aspects of this contribution centre on the fact that, for the first time, (i) a phase field theory explicitly incorporates the stored energy, and hence the dislocation densities generated during deformation, into the free energy function, and that (ii) a coupled constitutive framework is able to account for the static recovery-type mechanism responsible for the annihilation of dislocations in the wake of migrating grain boundaries. In the work presented in the 2D version of the coupled formulation, two phase field variables are relied upon to represent the microstructural characteristics of the mobile grain boundary, namely the crystallinity, η, and the grain orientation, θ. It is worth noting that the phase field model was formulated in 2D to enable the coupled formulation to be expressed using a simpler theoretical framework than in 3D. A simpler approach is first and foremost preferred for analytical and computational simplicity. Even though if only in-plane slip and lattice rotations can be considered in 2D, crystal plasticity simulations of 2D polycrystalline aggregates are known to provide accurate predictions of the plastic strain fields and slip activity and to be in qualitative agreement with 3D simulations, especially regarding the scaling between the stress and strain fields. Thus the stored energy distributions within each grain are comparable between 2D and 3D. As far as the phase field simulations are concerned, similar individual grain growth or shrinking rates and grain boundary mobility scaling with misorientations are expected in 2D and 3D, at least qualitatively. This is despite the fact that the grain boundary energy contributions involving the orientation and order parameter gradients (i.e. quadratic terms in the free energy function, see Equation (1) of Part I) are assumed to be isotropic. In contrast, different topological evolutions will occur in 3D due to the typically tetrakaidecahedral grain morphologies in polycrystals. This may affect, though not in a drastic way, the time-grain size scaling predictions to be discussed later in the text.

The predictive capabilities of the coupled formulation will be first validated by comparing its predictions against known analytical solutions and experimental data. To that purpose, simple validating examples will first be presented to show that some of the best well-known features of grain boundary migration phenomena in elasto-viscoplastic polycrystals are indeed captured by this approach. This will be followed by a discussion of finite element simulations of polycrystal behaviour and thermal recrystallisation phenomena. We believe that the present work, albeit applied to rather idealised examples at this stage, contains original phase field simulations of grain boundary migration coupled with stored energy induced by deformation, and with recovery.

The paper is organised in the following way. In Sections 2 and 3, the driving forces due to both curvature and stored energy are studied separately in order to ascertain their relative effects on grain boundary migration. First, the influence of misorientation is investigated in curved bicrystals where only the curvature is considered as a driving force for grain boundary motion. This is followed by the study of the evolving topology and kinetics of a polycrystal aggregate during grain growth. Then, the stored energy differences between grains in bicrystals with flat grain boundaries are examined. In Section 4, the thermal and dynamic recrystallisations of a high stacking fault energy material such as Al is investigated numerically. The key features of grain boundary motion of the model are discussed, and conclusions are presented in Section 5.

2. Curvature as a driving force

In this section, the effects of grain boundary misorientation on the boundary energy will be studied assuming that the boundary curvature is the only driving force for its migration, thus no stored energy is considered. Please refer to [16] for details about the formulation, finite element implementation and calibration of the coupled phase field-crystal plasticity formulation used in this work. The parameters of the phase field model used in the simulations are given in [16] with a few exceptions.

In this work, β_η and β_θ are the kinetic parameters of the phase field model, defined in Equations (36) and (37) of [16]. They control the time rate of change of the crystallinity and orientation order parameters, respectively, and ensure that no spurious grain rotations occur when the crystallinity variations are very small. They are assigned a temperature dependence through an inverse Arrhenius law involving an activation energy so as to recover the usual temperature dependence of grain boundary mobilities. This activation energy may be obtained from the measured mobility of specially misoriented grain boundaries (e.g. from low-Σ boundaries as in [16]). The specific values used in the simulations included in this work are $\beta_\eta = 0.01\,\mathrm{s}$ and $\beta_\theta = 100\,\mathrm{s}$ at 300°C. These values ensure that the curvature driven grain growth rate in pure aluminium exhibits the correct dependency on grain size and that the above spurious lattice rotations do not occur inside the grains. Further details about their calibration can be found in Sections 2.4 and 4.1.2 of [16].

The other phase field parameter which needs to be defined is e, defined in Equation (92) of [16], which controls the effective thickness of high angle grain boundaries (GBs) and hence their energies. A value of $e = 1.5 \cdot 10^{-2}\,\mathrm{J/m^3}$ will be used in the calculations unless otherwise specified.

2.1. *Effect of grain misorientation*

In the absence of stored energy, grain boundary motion can only occur in bicrystals with non-planar grain boundaries, thus a curved boundary will be considered here to investigate its behaviour in terms of the lattice misorientation between the grains. Consider a 2D circular grain of radius $R = 500\,\mu\mathrm{m}$ embedded in a much larger one. Here, Neumann boundary conditions are imposed on the crystallinity, η, and Dirichlet boundary conditions on the misorientation, θ. The results of the circular grain boundary migration behaviour for pure Al when the misorientation between the grains is 90° is given in Figure 1, which shows the grain boundary velocity versus boundary curvature obtained from experimental measurements [20] and the numerical predictions. It should be noted that, in this example, the shrinking of the grain results in a reduction of grain boundary area, thus the velocity of the circular grain interface is controlled by the decrease in the system free energy due to reduction of this grain boundary area. From the results in Figure 1, the grain boundary velocity, $\dot{R}$, can be seen to be proportional to the interface curvature, $1/R$, which is consistent with the experimental observations of Upmanyu et al. [20]. Then,

$$\dot{R} \propto \frac{M\,\gamma}{R} \tag{1}$$

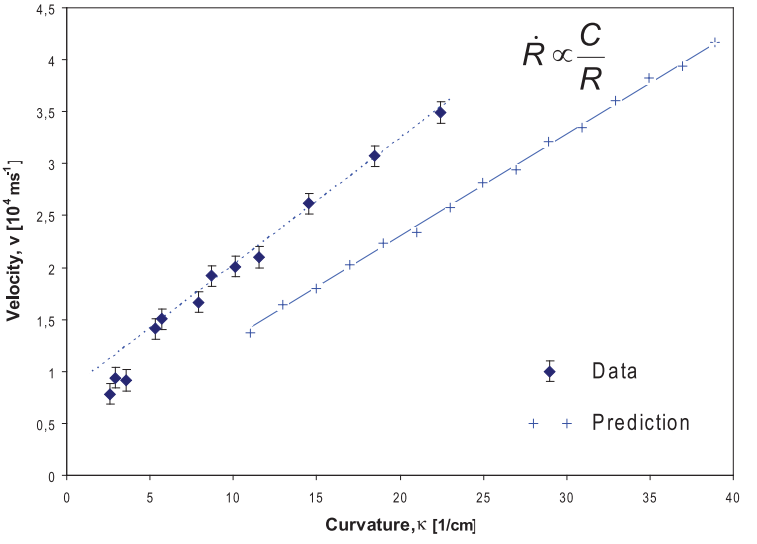

Figure 1. Experimental measurements [20] and numerical predictions of grain boundary velocity versus boundary curvature ($\kappa = 1/R$) for a general grain boundary in high purity Al having a 90° misorientation between the grains.

where M is the mobility and γ is the grain boundary energy (per unit area). It is worth pointing out that γ is associated with a surface and hence is expressed in J m^{-2}. However, its volume equivalent is the grain boundary energy density, $E_{gb} = \gamma/\delta$, where δ is a typical grain boundary thickness, and is expressed in J m^{-3}. Henceforth, E_{gb} will be generally used to maintain consistency of units with the stored energy due to deformation. This issue is discussed in more detail in [16]. Note also that, while the curvature of the grain boundary is a purely geometrical variable, its mobility and grain boundary energy are intrinsic material properties.

To investigate the effect of misorientation on the kinetics of the grain boundary, several misorientations between the grains were considered. To enable a comparison with available experimental data, Equation (1) may be expressed in terms of a reduced mobility, A_m, defined by the product of the mobility and the grain boundary energy, $A_m = M\ \gamma$. This reduced mobility calculated from the slope of the $\dot{R}$ versus $1/R$ curve for each misorientation is plotted in Figure 2. It can seen from this figure that the ability of grain boundaries (GB) to move depends strongly on the misorientation of the adjacent grains, in agreement with published experimental evidence (e.g. [7,21]). For larger misorientations typical of high angle GBs, the dependency of the GB mobility on misorientation weakens, eventually reaching a steady state value.

It is important to ascertain whether the phase field calculations can reproduce the known difference in mobilities of low and high angle GBs, which is attributed to the difference in the mechanism driving GB migration, i.e. involving dislocations in low angle GBs and atomic jumps in high angle GBs. A comparison between the FE and experimental results is given in Figure 3. Here, the relative mobility is defined as the ratio between the reduced mobility normalised by the reduced mobility's saturation value at large misorientations. It can be seen that both the experimental and

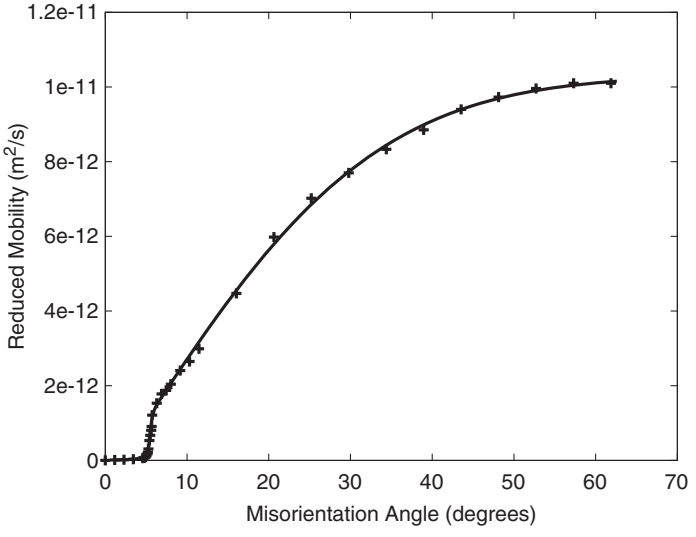

Figure 2. Reduced mobility dependency on grain boundary misorientation.

numerical results exhibit a degree of misorientation after which the mobility increases significantly, at approximately 11° in the experimental data (Figure 3a) and at 6° in the FE results (Figure 3b). The increase of the mobilities following these threshold misorientations seems also to be over a smaller range of misorientations in the numerical predictions.

Figure 4 compares the predicted mobilities with measurements reported in [31] corresponding to larger misorientations than those considered in Figure 3 at 300°C. It can be seen that the model is unable to describe the cusps observed at the Σ grain boundaries, as one would expect since the free energy function used in this work (see Figure 5 in [16]) does not include the well-known existence of cusps in the grain boundary energy versus misorientation curve. Nevertheless, Figure 4 shows that the saturated form assumed for the interface energy versus misorientation curve in Part I generally yields the correct monotonically saturating grain boundary mobility versus misorientation behaviour except for the special Σ grain boundaries. Note that this is a real model prediction since no special fit was performed to obtain the FE results of Figure 4.

2.2. *Topological evolution of polycrystalline aggregates*

The topological evolution of a 2D polycrystalline aggregate driven only by grain boundary curvature and triple junctions is discussed next. A representative volume consisting of an initial microstructure with 100 grains generated with a Voronoi algorithm and subject to periodic boundary conditions is considered. The initial grain orientations have been chosen randomly with the misorientation angle between neighbouring grains varying from 12° to 62°, as typically found in isotropic FCC polycrystals [23]. The aggregate is discretised using a finite element mesh made

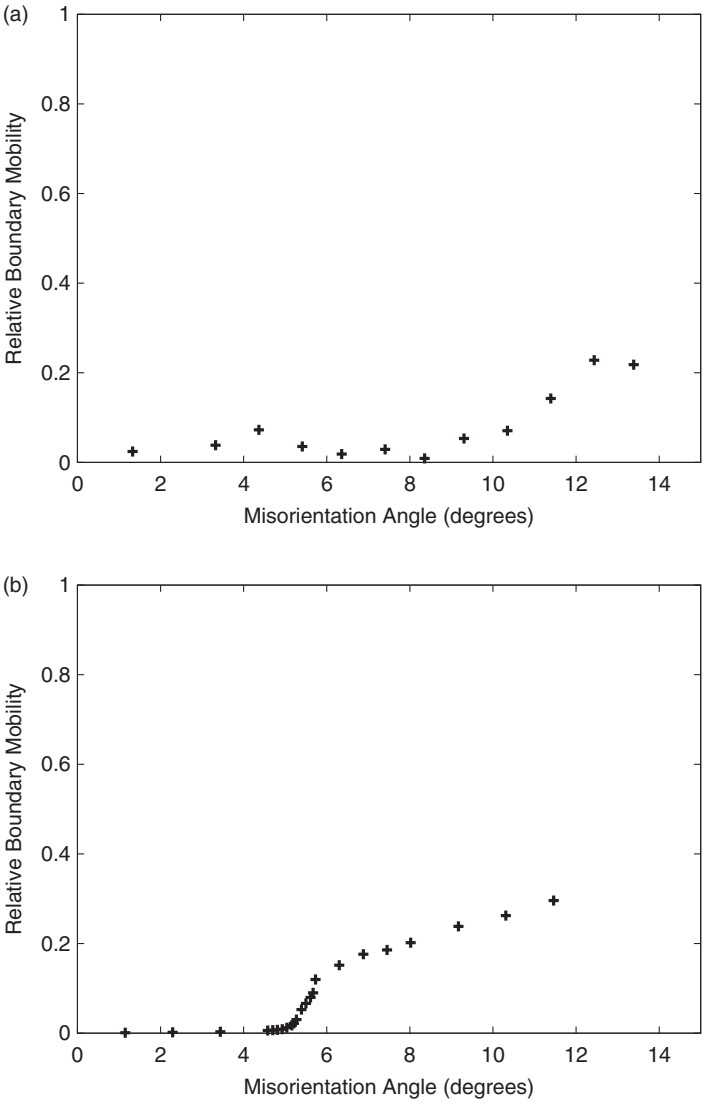

Figure 3. (a) Experimental [21] and (b) numerical variation of relative boundary mobility with misorientation angle.

up of 200×200 quadratic elements, and the annealing temperature is taken to be 315°C.

Figure 5 shows the predicted evolution of the microstructure as described by (a) the lattice orientation, θ, and (b) the lattice order, η. As expected, some grains grow in size and others vanish, resulting in a microstructure with a greater average grain size. Note that a comparison between the grain structures revealed by the contours of θ (Figure 5a) and η (Figure 5b) do not seem identical due to the fact that misorientations smaller than 10 degrees are not visible with the color scale.

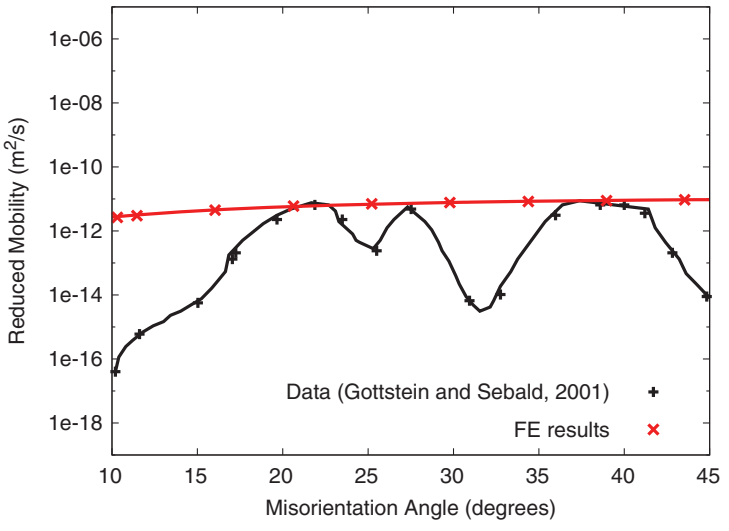

Figure 4. Comparison between experimental data [22] and numerically predicted reduced grain boundary mobility dependency on large grain boundary misorientations for pure Al at 300°C.

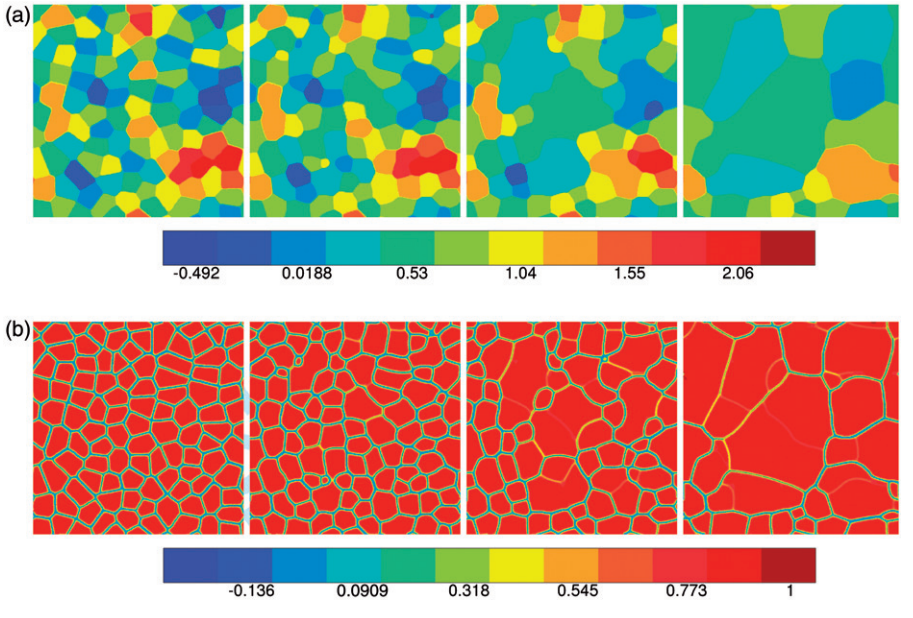

Figure 5. Predicted evolution of (a) grain orientation (θ) and (b) lattice order (η) contour plots. From left to right: $t = 0$, 18, 89, 2770 s.

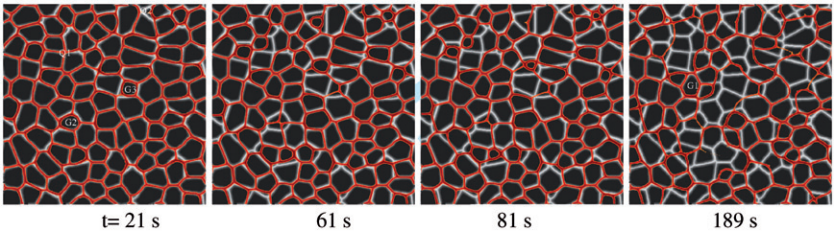

Figure 6. Superposition of the current (red line or grey line in the printed black and white version) and initial (white line) lattice order (η) regions where η is close to 0, at times 21, 61, 81 and 189 s.

However, low angle GBs are revealed by values of η near unity (i.e. with nearly perfect crystalline order) in light orange. In Figure 6, the topological evolution of the individual grain boundaries at different annealing times (21, 61, 81, 189 s) is compared to the initial grain boundary configuration. Recall that the GBs are identified by regions where the lattice order is $\eta \approx 0$. Here, the initial GB configuration is represented by the white contour lines, and the evolving GBs by the red ones.

The results presented in Figure 6 can be interpreted as follows. First, the triple junctions drag the boundaries when they are close to equilibrium. Most of the grains move slightly from their initial position to reach a pseudo-equilibrium, that is, respecting the dihedral law, and others disappear. For instance, the grains labelled G2 and G3 at $t = 21$ s quickly vanish at $t = 81$ s. Note that the dihedral angles obtained from this initial evolution are not necessary 120° due to the fact that the GBs possess different energies (i.e. they depend on the local misorientations). Once the triple junctions reach a configuration close to that required for thermodynamic equilibrium and the boundaries have obtained their required curvatures, the grain growth stage begins. Generally, the classical 2D theory of [24] and [25] predicts that grains with less than six neighbours will shrink while those with a greater number will grow. However, this theory is based on the assumption that all grain boundaries have equal mobilities and surface tensions. The approach proposed in this work is more general as it can take into account the different mobilities of low and high angle grain boundaries, as shown in Figure 3. Finally, note that in Figure 6 at $t = 189$ s, all grain boundaries have moved from their initial positions (white and red lines are nowhere superimposed). It can be seen that only one grain, labeled G1 at $t = 189$ s, remains close to its initial position. This grain exhibits six sides and dihedral angles close to 120°. An additional advantage of using lattice misorientations as a variable is that grain coalescence can naturally emerge from the calculations, as illustrated by the disappearance of junctions Q1 and Q2 at $t = 21$ s. Here, a new grain is formed from the two original ones which had relatively similar initial lattice orientations. Note that Q1 and Q2 are special cases of quadruple junctions. Grains containing this type of junction generally evolve by merging two of them. It can also be seen that the two grains merging at junction Q1 in Figure 5a were originally light black, thus having misorientations of less than 10 degrees. The same holds for the light green grains at junction Q2. The behaviour of such quadruple junctions are likely to evolve differently in 3D due to the more complex grain boundary topologies, thus the present 2D results offer mainly a qualitative understanding.

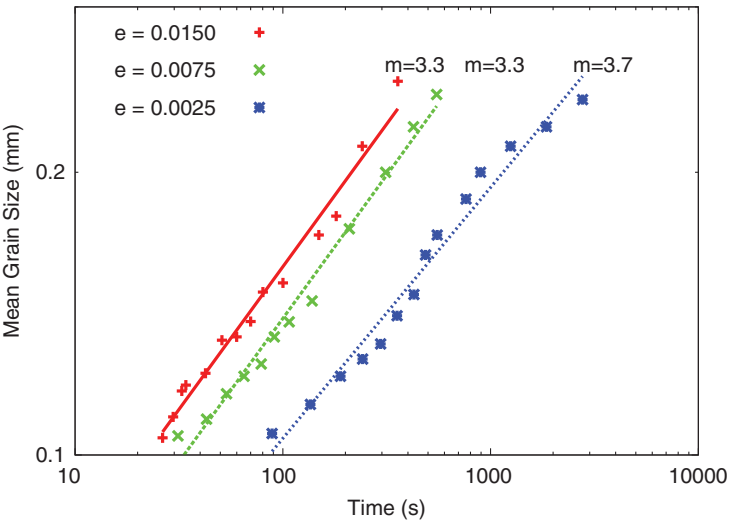

Figure 7. Linear interpolation of mean grain size versus time predicted behaviour for different values of the parameter e (given in J/m^3).

The number of grains considered in these simulations is probably too small to obtain reliable grain growth statistics. However, approximate macroscopic properties can be extracted from the numerical results so as to compare them with experimental data. It is also useful to assess parametrically the influence of the model parameter which controls the way in which the GB energy versus misorientation relation evolves for high angle GBs, viz. e in Equation (92) of [16], and hence the GB thickness. Figure 7 shows the evolution of the average grain size, $\overline{R}$, with time, t, for three different values of e. The predicted growth rate of the grain size can be approximated by a simple power law,

$$\overline{R} = Bt^{1/m}. \tag{2}$$

A linear fit to the numerical results (given by the symbols in Figure 7) yields growth exponents of $m = 3.3$ to 3.7 for values of e ranging from $1.5 \cdot 10^{-2}$ to $2.5 \cdot 10^{-3}\,J/m^3$, respectively. These values are larger than that of $m = 2.0$ obtained from the classical grain growth theory which, as previously discussed, does not account for the effect of misorientations in the GB energy and mobilitiy. However, experimental evidence on pure Al [26] reveals a growth exponent of approximately $m = 4.0$, which is closer to our predictions. Finally, Figure 7 also shows that the growth mechanism is delayed if the value of e decreases.

In order to gain an insight into the evolution of the grain orientations, Figure 8 shows the grain orientation distributions for the three different values of the parameter e at times when only 18 grains remain in each microstructure. Figure 8a reveals that the initial grain orientation distribution ranges mostly from 0° and 90° due to the defined misorientations between grains. The resulting microstructure obtained with $e = 1.5 \cdot 10^{-2}\,J/m^3$ is centred at $\theta = 40°$, while a greater spread in the

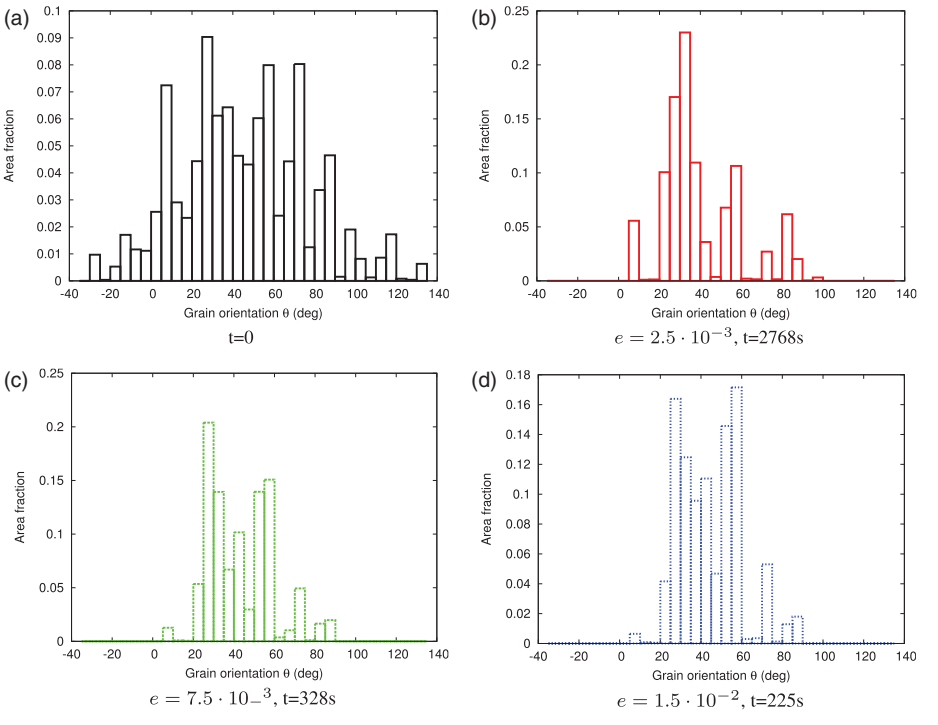

Figure 8. Grain orientation distributions (a) as defined initially at $t = 0$ s, and predicted at the times when only 18 grains remain in the aggregate for (b) $e = 2.5 \cdot 10^{-3}\,\mathrm{J/m^3}$, (c) $e = 7.5 \cdot 10^{-3}\,\mathrm{J/m^3}$ and (c) $e = 1.5 \cdot 10^{-2}\,\mathrm{J/m^3}$.

misorientation distributions can be found in the microstructures obtained with lower values of e. Finally, it is also worth noting that the microstructure obtained with $e = 2.5 \cdot 10^{-3}\,\mathrm{J/m^3}$ is more heterogeneous than the other distributions.

3. Stored energy as a driving force

3.1. *High angle grain boundary energy as an upper bound*

As explained in [16], in the phase field free energy formulation, the stored energy density, E_{st}, is normalised by the grain boundary energy density of interfaces exhibiting high angle misorientations, E_{hgb}. The normalised energy is then defined as $\bar{E}_{\mathrm{st}} = E_{\mathrm{st}}/E_{\mathrm{hgb}}$. The latter is assumed to be constant – thus no Σ grain boundaries are considered – and can then be regarded as an upper bound.

3.2. *Effect of stored energy on grain boundary velocity*

In this section, a bicrystal with a flat grain boundary is studied in order to suppress the curvature effect as a driving force for interface motion. The grains are misoriented by 40° and are assigned different values of stored energy due to

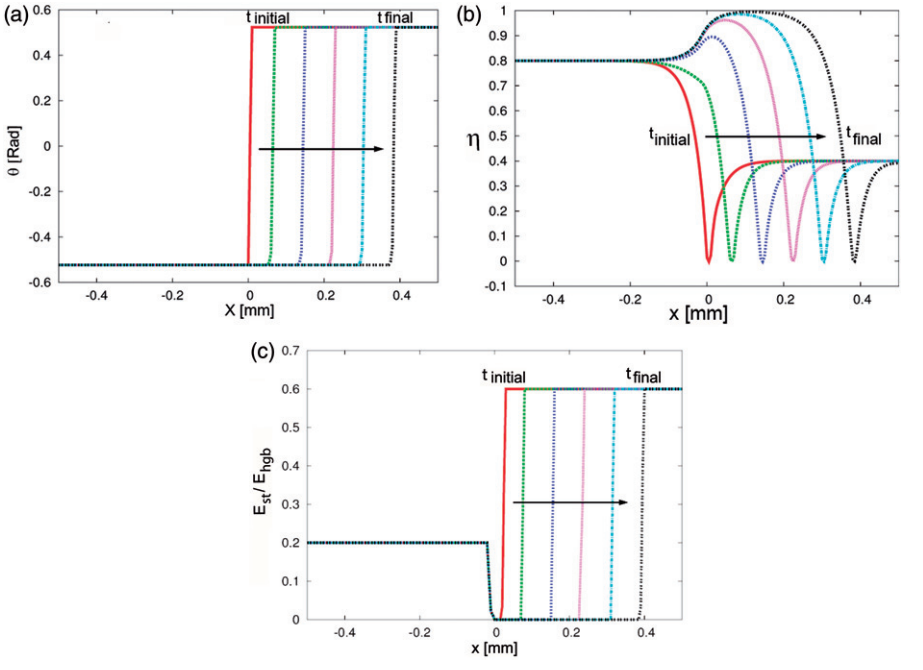

Figure 9. Simulation of a bicrystal interface driven by stored energy : (a) orientation, (b) crystallinity and (c) normalised stored energy distributions.

deformation, $\bar{E}_{st} = 0.4$ and 0.6, respectively, so as to introduce an energy gradient between both grains. The results are given in Figure 9, which shows how the grain boundary migrates towards the grain with the higher stored energy. It can be seen that the moving grain boundary leaves in its wake a crystal free of stored energy, where $E_{st} = 0$ and $\eta = 1$.

To study the effect of the stored energy gradients on the grain boundary velocity, several flat grain boundaries with different stored energy gradients were considered using different values of the relaxation parameter, β_η. The results are given in Figure 10a in terms of the GB velocity versus the stored energy difference at 300°C for three different values of β_η. These results yield a linear relationship between the driving force arising from stored dislocations and the grain boundary velocity. Such linearity has also been reported in the experimental work of [27], as shown in Figure 10b. Note also that the critical stored energy is higher for the inverse mobility parameter, $\beta_\eta = 10^{-1}$ s. Since β_η controls the evolution of the phase field variable η, its variation affects the annihilation rate. However, as seen in Figure 10a, the results for $\beta_\eta = 10^{-2}$ s and $\beta_\eta = 10^{-6}$ s are similar. This observation leads to the conclusion that, for a given value of β_θ, there is a threshold value of β_η below which it no longer has any effect on the grain boundary velocity. Nevertheless, to avoid spurious grain rotation [19], $\beta_\theta \gg \beta_\eta$ so that there is a narrow range of suitable β_η values which gives the desired GB velocity while inhibiting grain rotation. Here, this range was found to be 10^{-1} s and 10^{-2} s for the value of $\beta_\theta = 100$ s. Thus, the impact of the inverse mobility parameter, β_η, on the GB velocity is rather limited, while the inverse

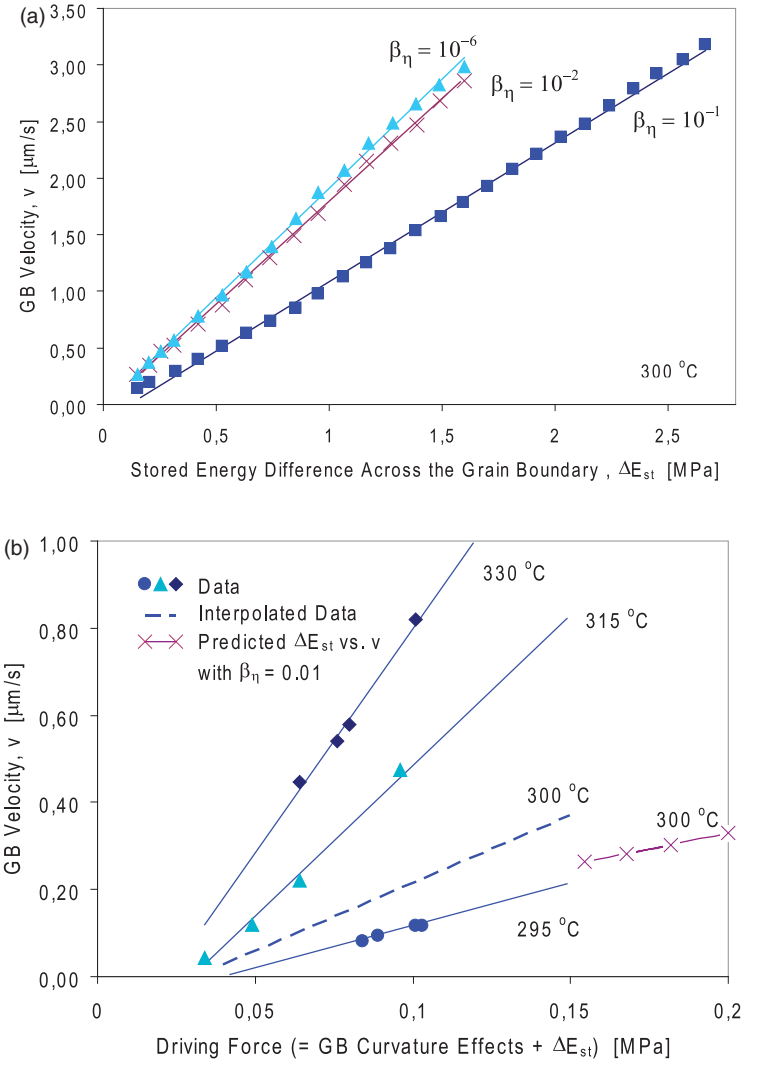

Figure 10. Relation between the boundary velocity and its driving force in pure Al: (a) numerical predictions at 300°C, and (b) comparison between the experimental data in the 295–330°C temperature range [27] with the predictions from $\beta_\eta = 0.01$ s case of (a).

mobility parameter, β_θ, serves as the main adjusting parameter to match the experimental data. Figure 10b also includes for comparison the numerical predictions at 300°C reported in Figure 10a for the $\beta_\eta = 10^{-2}$ s case. It can be seen that the 300°C predictions compare reasonably well with the data at that temperature, which is encouraging in view of the fact that the simulations were carried out assuming flat grain boundaries in contrast to the curved boundaries of the actual material from which the measurements in Figure 10b were obtained.

Figure 11 shows the GB velocity versus the normalised difference in stored energy for different values of the parameter e used to define the high angle grain boundary

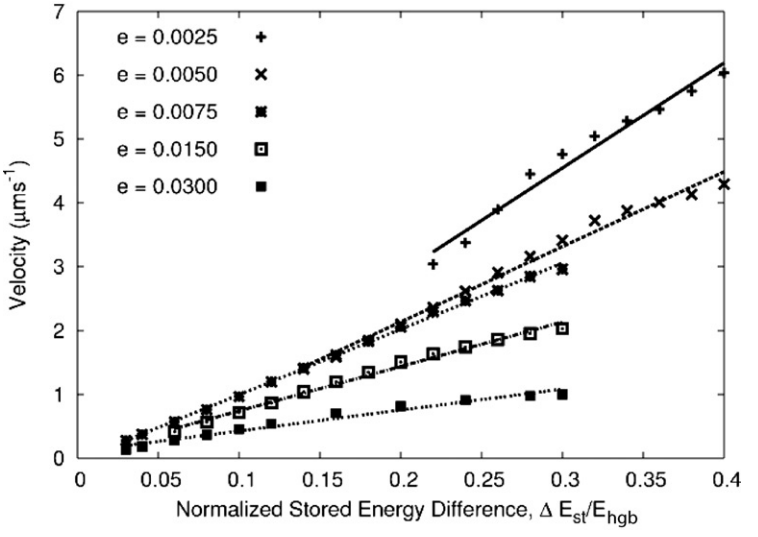

Figure 11. Predicted dependence of the grain boundary velocity on the normalised difference in stored energy for different values of the parameter e.

energies (recall that an increase in e increases the thickness of the grain boundary). It can be seen that the predicted trend is linear, as in Figure 10a, and that the slopes of the lines increase with decreasing values of e. It can also be noted that the threshold value of the stored energy difference between both grains required to trigger or activate grain boundary motion decreases with increasing e. These results show that, for instance, $\Delta\bar{E}_{\mathrm{st}} = \Delta E_{\mathrm{st}}/E_{\mathrm{hgb}} = 0.03$ when $e = 7.5 \cdot 10^{-3}\,\mathrm{J/m^3}$ and $\Delta E_{\mathrm{st}}/E_{\mathrm{hgb}} = 0.23$ when $e = 2.5 \cdot 10^{-3}\,\mathrm{J/m^3}$.

4. Combined effect of curvature and stored energy

4.1. *Growth of nuclei*

Nucleation plays a major role in determining both the size and orientation of the grains in the final microstructure. Two main nucleation mechanisms have been reported: classical nucleation and strain induced boundary migration (SIBM). In classical nucleation, grain nuclei originate from small volumes of the lattice which have accumulated high enough levels of stored energy during previous deformation to force the lattice to reorient itself [1,28]. Here, the newly formed nuclei are highly misoriented with respect to the deformed lattice from which they originate. In contrast, in SIBM the new grains have similar orientations to those from which they have grown. It involves the bulging of part of a pre-existing grain boundary, leaving a region behind the migrating boundary with a lower dislocation content. The SIBM mechanism, identified first by [29], dominates at low levels of deformation whereas the classical nucleation does so at higher levels. For instance, in pure aluminium, SIBM is observed only at deformations of less than 40%. However, in this work a weakly deformed microstructure will be assumed (around 15%) so that the lattice

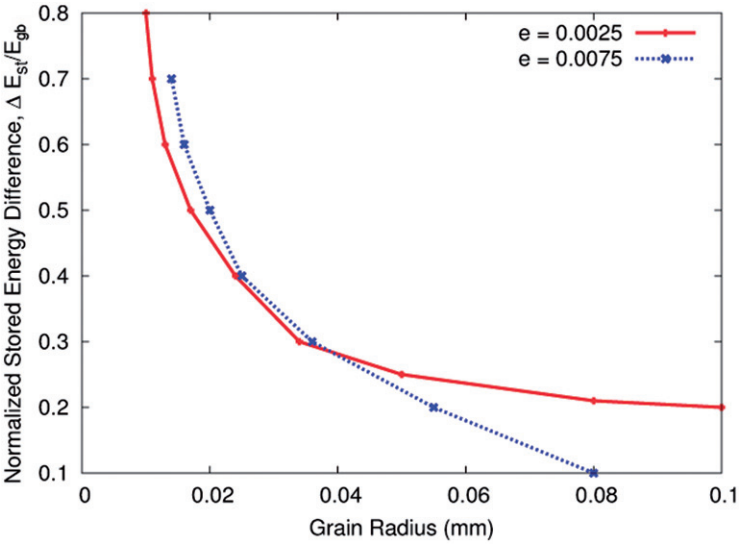

Figure 12. Predicted dependency of the critical stored energy for grain growth on the initial nuclei size.

orientation within each grain is approximately constant. Hence, in this work SIBM will be considered to be the only active recrystallisation mechanism. Since, in the SIBM new grains have orientations similar to those of the old grains from which they have grown, a simple approach is to consider that the new grains have similar orientations to the original ones.

In Section 2.1, the evolution of a circular grain embedded within a larger one was investigated when this process was driven just by the GB curvature and energy. It was shown that the circular grain gradually decreased in size and then vanished. Next, it will be shown that when the combined effects of grain boundary curvature and stored energy are accounted for, it is possible to simulate the growth of a small nucleus or seed located inside a deformed microstructure up to a thermodynamically stable configuration. In this case, the difference between the energy stored in the deformed grain, containing a well developed dislocation structure, and that of the nucleus, free of dislocations, constitutes the additional driving force.

Consider a small nucleus free of dislocations, that is with $\bar{E}_{st} = 0$, embedded in a deformed grain with a relative stored energy of $\bar{E}_{st} = 0.8$. Dirichlet boundary conditions are applied on the top and right sides of the model. The predicted growth of the initial nucleus revealed that, after migrating toward a higher stored energy region, the grain boundary leaves in its wake a region free of dislocations and hence stored energy. Note that the nucleus grows only if a sufficient amount of stored energy exists in the matrix for the assumed initial size of the nucleus. To determine the critical amount of stored energy required to obtain grain growth, simulations were performed using different values of stored energy and initial nuclear sizes. The resulting critical stored energy versus initial size of nucleus are given in Figure 12 for two different values of the parameter e. The predicted trend is as expected: the

smaller the initial grain size, the greater the amount of stored energy needed for grain growth to occur. Note also that the required initial grain size is relatively large, ranging from 10 to 100 μm. However, these values depend on the parameter e, which defines the thickness of the GB, and on the mesh size. A mesh sensitivity study on a similar simple model can be seen in [30].

4.2. *Nucleation and recrystallisation: stored energy effects*

In this section, the combined effects of GB curvature and stored energy on the microstructural evolution of a polycrystalline aggregate during thermal recrystallisation is investigated. The initial morphology of the initial 2D aggregate and boundary conditions are identical to those defined in Section 2.2. The initial values of the grain orientation field variable, θ, is also assigned in a similar way as before, that is, randomly with the misorientation angles between neighbouring grains varying from 12° to 62°, see Figure 13a at $t=0$. The parameter e is taken as 0.0025, and the initial distribution of the stored energy is assumed to vary between 0 and $0.40E_{\mathrm{hgb}}$, depending on the value of θ assigned to each grain. Here, it is assumed rather arbitrarily that grains with the highest values of θ will be able to store less strain energy. The resulting initial distribution of the normalised stored energy is given in Figure 13c at $t=0$. Finally, the initial intra-granular value of the lattice order is made to depend on the stored energy according to the relation introduced by Equation (42) of [16], namely

$$\eta = 1 - \bar{E}_{\mathrm{st}} \frac{C_e}{\omega^2}, \tag{3}$$

where C_e is a parameter which must satisfy the relation $C_e \leq \omega^2/\bar{E}_{\mathrm{st}}$. Here, it is assumed for convenience that $C_e=\omega^2$, which implies that the theoretical upper bound for E_{st} is the high angle grain boundary energy, E_{hgb}. It should also be recalled that for this case, the corresponding value of η is that of a fully disordered lattice, viz. $\eta=0$.

Figure 13b at $t=0$ gives the resulting initial distribution of η defined as per Equation (3). It can be seen that the initial lattice order distribution accounts for the disorder introduced by the dislocation structures developed during deformation, represented by the stored energy, and that $\eta<1$ inside the grains. Here, the lighter colour grains (yellow) exhibit a greater level of disorder, since they have stored more strain energy, than the darker ones (red).

The subsequent evolution of the microstructure during thermal recrystallisation at 315°C at times 9, 28 and 167 s is shown in the contour plots of Figures 13a–c for θ, η and $\bar{E}_{\mathrm{st}}$, respectively. It may be noted that the grain boundaries move first through areas where the stored energy is the greatest and that grains with the highest initial stored energies (labelled R1-10 in (b) at $t=0$), eventually vanish completely. Thus the inclusion of the stored energy term in the phase field's overall free energy expression promotes the evolution of grain orientations toward grains having the lowest values of stored energy.

The evolution of the recrystalised regions can be identified through the grains which have no stored energy left. The corresponding recrystallised regions are shown

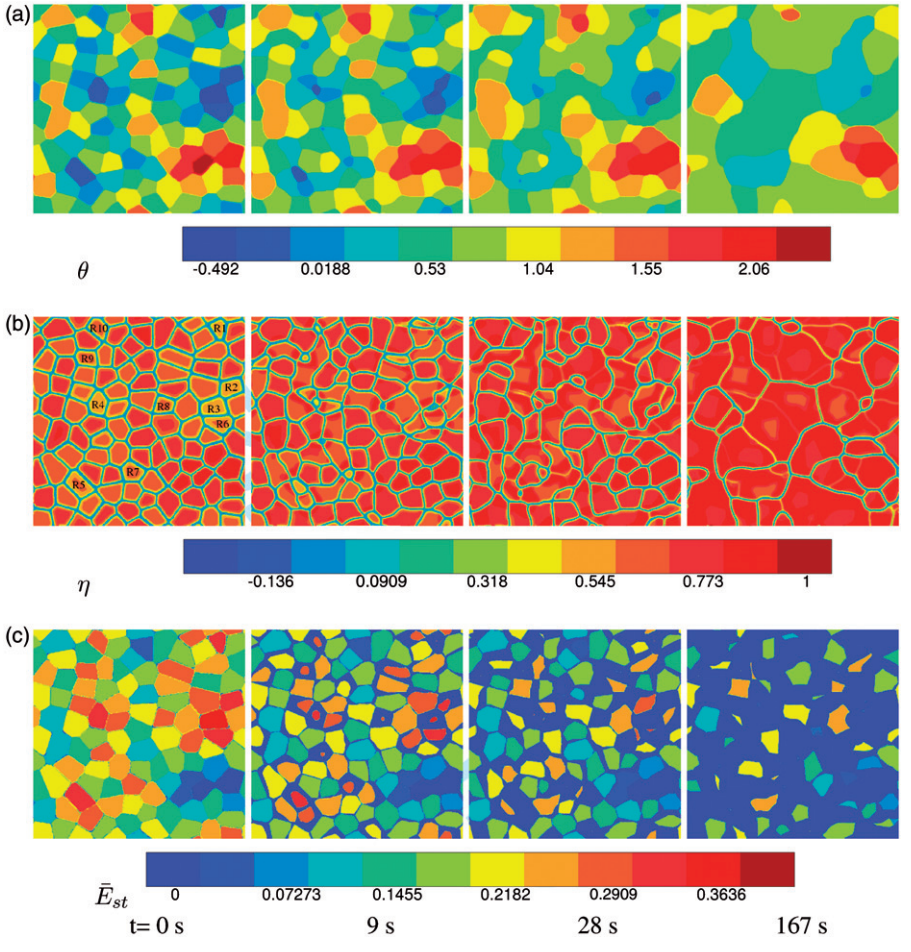

Figure 13. Predicted evolution of the polycrystalline aggregate microstructure during thermal recrystallisation at 315°C at times 0, 9, 28 and 167 s, shown as contour plots of (a) the grain orientation variable, θ, (b) the lattice order variable, η, and (c) the normalised stored energy, $\bar{E}_{\mathrm{st}}$.

in Figure 14 at times 0, 1.5, 14 and 60 s. Here, the red (light) regions describe the recrystalised grains, and the black (dark) ones the deformed matrix. It is worth noting that in the last contour plot, at $t = 60$ s, some grains have not yet recrystallised thus there is still a certain amount of stored energy left in the microstructure. By comparing these grains with the same ones in Figure 13c, it can be seen that the unrecrystalised grains correspond to those with low values of initial stored energy. In these grains, the threshold stored energy difference required to activate the motion of the grain boundary has not been reached thus no grain boundary has moved through them.

To understand the kinetics of recrystallisation, the volume fraction of recrystallised material, X_v, has been extracted from the FE results as a function of time. The results are shown in Figure 15a in terms of X_v and the annealing time, with

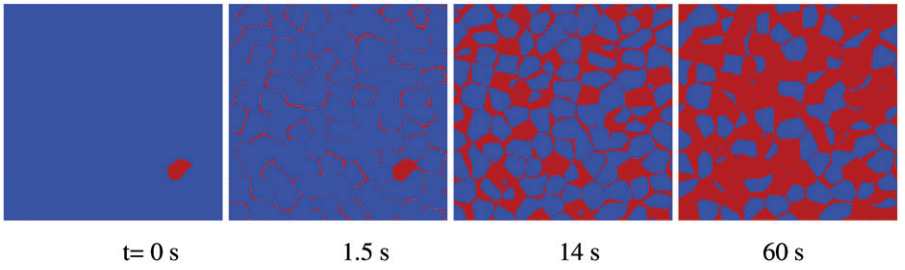

Figure 14. Evolution of the recrystallised regions in the aggregate at $t = 0$, 1.5, 14 and 60 s: unrecrystalised regions are in black and recrystallised ones in red.

the latter plotted in a logarithmic scale. The resulting curve exhibits the standard S shape of most transformation kinetics problems, which is usually well described by the following function,

$$X_v = 1 - \exp(-Bt^n). \tag{4}$$

The calibration of the parameters B and n can be done based on the linear part of the X_v versus $\log(t)$ curve in Figure 15a. The results are given in Figure 15b, which shows that the fitted value of the coefficient n is 0.88, which compares well with the experimental value of $n = 1.0$ reported by [26]. A value of $B = 0.01$ $1/s^n$ was found from the results presented in Figure 15b. Bearing in mind that $1/B$ provides an estimate of the transient time for recrystalisation to be completed when n is close to unity, it can be seen that the predicted value of $1/B = 100$ s is consistent with the results shown in Figure 15a. A comparison was made between these predictions and the experimental work published by Liu and Morris [31] on a cold rolled AA 5182 aluminium alloy. Based on the measured variations in hardness with annealing time at different temperatures, they found the measured recrystalisation kinetics at 300°C to be approximately 200 s, in reasonably good agreement with the predicted 100 s, specially bearing in mind that the predicted results are for pure aluminium. The measured value of the exponent n reported in [31] ranged from 1.7 to 2.1, which contrasts with the value of $n = 0.88$ predicted here, albeit for pure aluminium, which may explain the discrepancy.

4.3. *Dynamic recrystallisation*

So far, we have considered grain nucleation and growth driven by the energy stored during previous deformation and GB curvature. Next, the microstructural evolution of a 2D Al polycrystalline aggregate will be considered while it undergoes a 1% reduction in height. Thus the microstructure will evolve in a similar manner as during dynamic recrystallisation. The stored energy associated with the evolving dislocation structure is determined from the crystal plasticity calculations (see [16]). For simplicity, the aggregate is assumed to be made up of 10 grains, and the initial lattice orientation of each grain required for the crystal plasticity calculations are assumed to be homogeneous and given by the initial values of the phase field

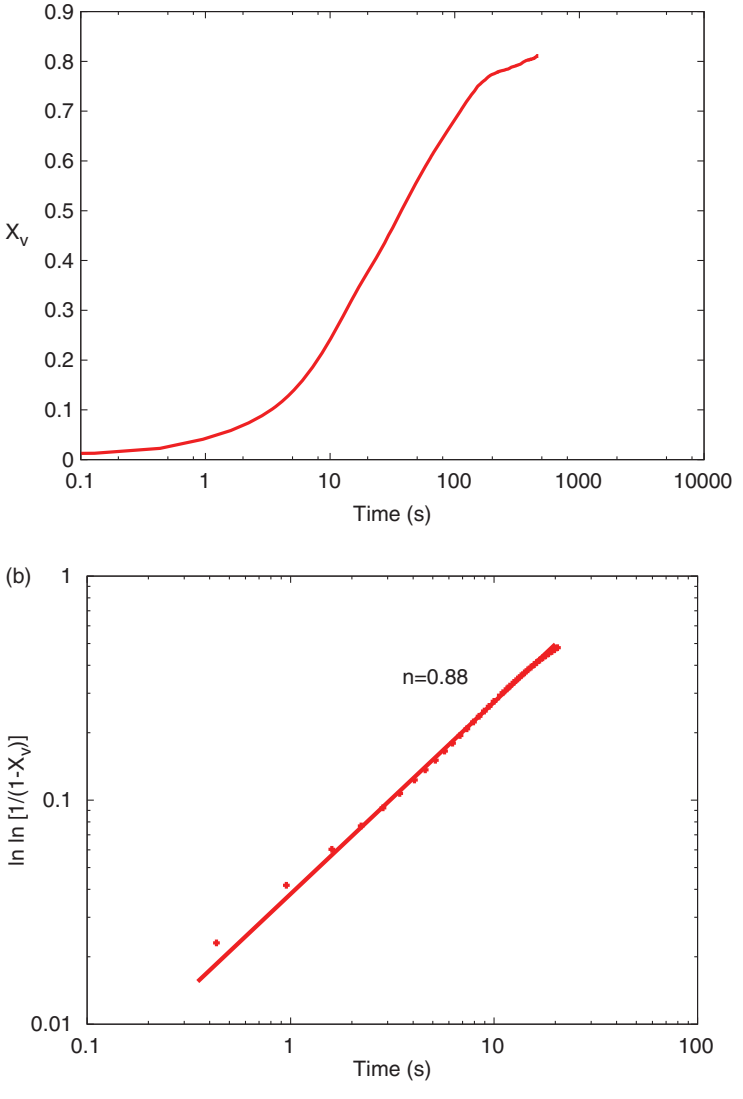

Figure 15. (a) Evolution of the predicted fraction of the recrystalised microstructure, X_v, with respect to time, and (b) fitting of the exponent n in Equation (4) to the linear part of (a).

variable, θ. Therefore, instead of having sharp grain boundaries, they will be assumed to have a finite thickness due to the diffusive nature of θ in these regions.

In this example, the stored energy generated by the deformation itself is updated from the dislocation densities predicted by the evolutionary equations of the single crystal model. The numerical results are shown in Figure 16, which give the microstructural evolution of the aggregate at different times during the 1% compression test in terms of distributions of (a) the orientation, θ, and (b) the Mises stress. It can be seen that the results reveal similar changes in morphology in the recrystalising microstructure as in the larger polycrystal aggregate discussed

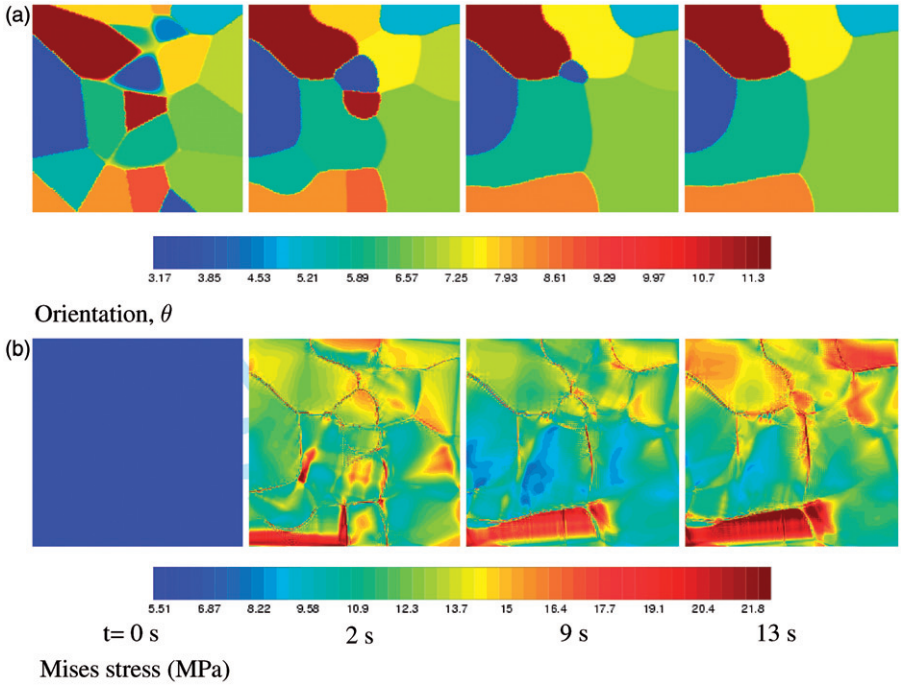

Figure 16. Example of a coupled phase field-crystal plasticity analysis: distributions of (a) grain orientation, θ, and (b) equivalent Mises stress at times 0, 2, 9, and 13 seconds in a small 2D aggregate undergoing a 1% compression at 300°C.

earlier in the text. It is also worth noting the effect of the finite grain boundary width on the local stresses, even though they are relatively low in magnitude (as expected in pure Al at 300°C). The stresses concentrate around this region in a similar way as do the local internal stresses which develop near grain boundaries by deformation incompatibilities or dislocation pile-ups. Ongoing work on a larger aggregate to study in more detail the local GB fields will be reported in a future publication.

5. Concluding remarks

The capabilities of the coupled constitutive framework proposed by [16] to describe the evolution of a polycrystalline microstructure driven by grain boundary curvature and/or stored energy has been investigated. Several examples of microstructural evolution involving grain boundary migration have been addressed. First, the study of a bicrystal with only curvature as the driving force for boundary migration revealed the ability of the model to reproduce the known difference in mobilities between low and high angle grain boundaries, including the threshold misorientation below which the mobility is negligible. Nevertheless, further developments on the current grain boundary energy formulation are required to incorporate the description of the grain boundary mobility cusps observed at Σ-type boundaries.

A linear relation between the velocity and grain curvature was also predicted, in accordance with reported experimental trends. Then, an example involving a small dislocation-free circular grain or nucleus embedded within a highly deformed one, thus having both curvature and stored energy as competing driving forces, was relied upon to study the growth of stable nuclei. One important finding was that the threshold level of stored energy necessary for grain growth to start was found to increase nonlinearly with the initial size of the nucleus.

The important role of strain induced boundary migration in high stacking fault energy materials, such as Al where recrystallisation twinning is not important, was also investigated. Here, the role of the existing subgrain or cell structures was accounted for through the average local dislocation densities, and the corresponding stored energies. The study of thermal recrystallisation and grain growth phenomena in pure aluminium relied on a 100 grain representative polycrystal aggregate. Although this number of grains may not be considered as statistically representative, the model has been shown to be capable of predicting the basic features of thermal recrystallisation, including nucleation phenomena and grain growth. For instance, the results have clearly confirmed that grains with the lowest stored energy are dominant at the end of the recrystallisation process. In spite of the complexity of the formulation and the processes involved, some of the predictions were found to be in good agreement with the experimental evidence, such as the predicted evolution of the recrystallised material volume fraction with respect to time and the predicted kinetics of recrystallisation and grain growth. An example involving dynamic recrystallisation was considered to illustrate the coupling between the grain boundary kinematics and the dislocation densities determined from crystal plasticity. The polycrystal studies also enabled us to gain an understanding of the effect of the grain boundary energy parameters and the initial lattice orientations on the width of the diffuse grain boundaries. They were found to be rate-controlling in that they affect the microstructure evolution and the resulting grain orientations.

In summary, the proposed coupled phase field-crystal plasticity formulation has yielded encouraging results in the study of grain growth and recrystallisation. However, there are many features still to be improved and investigated such as a better description of physical properties (e.g. anisotropy in the phase field), nucleation phenomena, effects of grain dislocation substructures, and 3D phenomena.

Acknowledgements

This research was supported by the European Commission, project DIGIMAT (contract number NMP3-CT-2006-017105). This support is gratefully acknowledged.

References

[1] F. Humphreys and M. Hatlerly, *Recrystallization and Related Annealing Phenomena*, Pergamon Press, Oxford, 2004.
[2] V. Erukhimovitch and J. Baram, Mater. Sci. Eng. A 214 (1996) p.78.
[3] M. Crumbach, M. Goerdeler and G. Gottstein, Acta Mater. 54 (2006) p.3275.
[4] O. Ivasishin, S. Shevchenko and S. Semiatin, Acta Mater. 57 (2009) p.2834.

[5] D. Zöllner and P. Streitenberger, Scripta Mater. 54 (2006) p.1697.
[6] V. Marx, F. Reher and G. Gottstein, Acta Mater. 47 (1999) p.1219.
[7] G. Gottstein, D. Molodov, L. Shvindlerman, D. Srolovitz and M. Winning, Curr. Opin. Solid State 5 (2001) p.9.
[8] J. Geiger, A. Roosz and P. Barkoczy, Acta Mater. 49 (2001) p.623.
[9] S. Gill and A. Cocks, Acta Mater. 44 (1996) p.4777.
[10] L. Barrales Mora, G. Gottstein and L. Shvindlerman, Acta Mater. 56 (2008) p.5915.
[11] S. Osher and J. Sethian, J. Comput. Phys. 79 (1988) p.12.
[12] L. Chen and D. Fan, J. Amer. Ceram. Soc. 79 (1996) p.1163.
[13] S. Biswas, I. Samajdar, A. Haldar and A. Sain, J. Phys.: Condens. Matter 23 (2011) p.172.
[14] A. Mallick and S. Vedantam, Comput. Mater. Sci. 46 (2009) p.21.
[15] D. Raabe and R. Becker, Model. Simul. Mater. Sci. Eng. 8 (2000) p.445.
[16] G. Abrivard, E.P. Busso, S. Forest and B. Apolaire, Phil. Mag. (2012) (this issue).
[17] Y. Suwa, Y. Saito and H. Onodera, Mater. Sci. Eng. A 457 (2007) p.132.
[18] T. Takaki, Y. Hisakuni, T. Hirouchi, A. Yamanaka and Y. Tomita, Comput. Mater. Sci. 45 (2009) p.881.
[19] G. Abrivard, *A coupled crystal plasticity – phase field formulation to describe microstructural evolution in polycrystalline aggregates during recrystalisation*, PhD thesis, Ecole des Mines de Paris, 2009.
[20] M. Upmanyu, D. Srolovitz, L. Shvindlerman and G. Gottstein, Acta Mater. 47 (1999) p.3901.
[21] C. Yang, A. Rollett and W. Mullins, Scripta Mater. 44 (2001) p.2735.
[22] G. Gottstein and R. Sebald, J. Mater. Process. Technol. 117 (2001) p.282.
[23] J.K. Mackenzie, Acta Metall. 12 (1964) p.223.
[24] J. Von Neumann, *Discussion – shape of metal grains*, in *Metal Interfaces*, C. Herring, ed., American Society for Metals, Cleveland, OH, 1952, p.108.
[25] W. Mullins, J. Appl. Phys. 27 (1956) p.900.
[26] P. Gordon and T. El-Bassyouni, Trans. Metallurg. Soc. AIME 223 (1965) p.391.
[27] Y. Huang and F. Humphreys, Acta Mater. 47 (1999) p.2259.
[28] E.P. Busso, Int. J. Plasticity 14 (1998) p.355.
[29] P. Beck and P. Sperry, J. Appl. Phys. 21 (1950) p.150.
[30] K. Ammar, B. Appolaire, G. Cailletaud, F. Feyel and S. Forest, Comput. Mater. Sci. 45 (2009) p.800.
[31] W. Liu and J. Morris, Mater. Sci. Eng. A 402 (2005) p.215.